Journal of Membrane Science 476 (2015) 311–320

Contents lists available at ScienceDirect

Journal of Membrane Science

journal homepage: www.elsevier.com/locate/memsci

# Scale-up characteristics of membrane-based salinity-gradient power production

Benjamin J. Feinberg [a], Guy Z. Ramon [b], Eric M.V. Hoek [a,*]

[a] Department of Civil & Environmental Engineering, Institute of the Environment & Sustainability, California NanoSystems Institute, University of California, Los Angeles, CA, USA

[b] Department of Civil & Environmental Engineering, Technion – Israel Institute of Technology, Haifa, Israel

ARTICLE INFO

*Article history:*
Received 20 May 2014
Received in revised form
8 October 2014
Accepted 10 October 2014
Available online 18 November 2014

*Keywords:*
Salinity gradient power
Pressure-retarded osmosis
Reverse electrodialysis
Renewable energy

ABSTRACT

The controlled mixing of streams with different salinity is a potential route for clean and renewable base-load power generation. Here, a comprehensive process model has been developed for pressure-retarded osmosis (PRO) accounting for full-scale system losses such as viscous dissipation, external mass transfer and equipment efficiency. Also, an existing model for reverse electro-dialysis (RED) is adapted to account for analogous full-scale system losses. The models are used to predict practical power densities and process efficiencies. The projected power density for PRO (using best available membranes) is much lower than generally predicted by extrapolation of experimental data. For example, a power density of 4 W/m$^2$ extrapolated from laboratory experiments actually yielded negative power at full-scale. The maximum power density for PRO is doubled as the hydraulic energy recovery (HER) efficiency is increased from 90% to 99%. Furthermore, the operating pressure, load voltage, and crossflow velocities typically applied in laboratory studies appear much too high to be practical in full-scale PRO and RED systems. Notably, RED systems exhibit a lower system size required for achieving a given degree of mixing, compared with PRO. For both processes, maximum energy efficiency does not occur at thermodynamic equilibrium due to hydraulic losses. Finally, maximum power density appears to be an inadequate parameter for assessing full-scale PRO/RED process feasibility because both processes could produce the same maximum power density, yet exhibit different power outputs and efficiencies and system sizes.



## 1. Introduction

Clean, renewable energy may be produced by controllably mixing streams of different salinity [1,2]. This is achieved by employing membranes that facilitate selective transport of either solute or solvent, resulting in different process characteristics with various advantages and disadvantages. Pressure-retarded osmosis (PRO) and reverse electro-dialysis (RED), the two most popular salinity gradient power (SGP) technologies, are discussed in detail in the literature (see, for example, Refs. [1,3–9]). While both PRO and RED involve mixing dilute and concentrated solutions, the energy conversion mechanism achieved via mixing is fundamentally different. PRO involves the diffusion of water molecules across a semipermeable membrane from a dilute feed stream into a pressurized concentrated stream, augmenting its volume upon dilution. The volume-augmented feed is then passed through a hydro-turbine where the mechanical energy is converted into electricity. RED involves the diffusion of salt ions across charge-selective ion exchange membranes, creating an ionic flux that is converted into an electron flux at an electrode surface, and power is harnessed through an applied load in an external circuit.

Previous modeling work on SGP technologies has focused on the maximum power density produced through PRO or RED. However, maximum power density alone is an insufficient metric for designing a large-scale, realistic SGP system. Even in an ideal system, maximum power density will only be achieved at the system inlet where the concentration gradient is the largest, but downstream mixing of the streams inevitably lowers the power density. Conversely, energy efficiency, defined as the ratio of produced-to-available energy, is maximized at the point of complete mixing, which would theoretically occur at the system outlet. However, complete mixing would require infinite system size (or residence time). Therefore, in order to evaluate the scale-up of SGP technologies, it is essential to first understand how system-level power density and energy efficiency (and therefore total power output) change with module length (a proxy for system size).

* Corresponding author. Current address: Water Planet Engineering, 721 S. Glasgow Avenue, Suite D; Los Angeles, CA, USA. Tel.: +1 424 331 7701; fax: +1 424 331 7799.
*E-mail address:* eric@waterplanet.com (E.M.V. Hoek).

http://dx.doi.org/10.1016/j.memsci.2014.10.023
0376-7388/

A full-scale process model accounting for changes in velocity, pressure, and concentration along the length of the flow channels can provide a direct, quantitative indication of these important process metrics. To the best of our knowledge, a detailed process model has yet to be published for PRO. For RED, a potentially full-scale process model has already been proposed [10]; however, it was employed for the purpose of comparison with experimental measurements on a small-scale system and was not used to evaluate full-scale performance. Moreover, the model did not consider external mass transfer, which significantly impacts the performance at low crossflow velocity [2]. A recent study by Vermaas et al. applied a process model to evaluate changes in energy recovery and power density over relatively short lengths, but did not account for membrane resistance, viscous dissipation, or concentration polarization [11]. Furthermore, detailed comparisons of PRO and RED previously published have considered the maximum power density achievable, but did not consider how both energy efficiency and average power density would comparatively scale with system size.

The purpose of this paper is to identify how full-scale performance varies with the main process parameters. In particular, this is the first time that PRO performance has been evaluated by a full-scale process model. Note that the two processes modeled are envisioned with different system dimensions and operating principles; hence, directly comparing PRO and RED is naturally a difficult task. Therefore, the results presented herein are designed to illustrate the potential of a full-scale process model and the extension of that model to practical scale-up considerations. The results are not intended to be a prescriptive statement on which process is technologically superior. Furthermore, although PRO and RED can be envisioned as multi-stage processes, we only consider a single stage (single hydro-turbine and single electrode for PRO and RED, respectively). Finally, only co-current cases are considered here; cross-current or counter-current configurations could produce different results.

## 2. Model formulation

In this section, one-dimensional process models are developed for both PRO and RED, in the spirit of previous efforts to model full-scale reverse osmosis systems [12–15]. In this framework, cross-sectional variations of velocity and concentration in the flow channels are not explicitly solved. Instead, mass transfer correlations are used to account for external concentration polarization (in the case of PRO, internal concentration polarization is accounted for as well), and a friction factor is used to account for viscous dissipation. This results in a significant computational simplification, producing a coupled system of non-linear ordinary, rather than partial, differential equations. Through employing this flexible approach, operational parameters can be more rapidly adjusted and evaluated over a wider range as compared with more computationally intensive approaches such as computational fluid dynamics (CFD). The one-dimensional model is the first step toward approximating scale-up of salinity gradient energy and requires much less computational power than more complex modeling techniques. While over short lengths CFD can be of great use, over longer system lengths (many meters) it is not computationally rational to apply two- and three-dimensional approaches. We note that good correlation between one-dimensional models and experimental data has been reported in the past for the fouling of reverse osmosis systems [16]. In the present formulation, other inefficiencies are included, such as co-ion transport and salt leakage, hydraulic losses within the module, and machine inefficiencies (pumps, hydro-turbine, hydraulic energy recovery device).

Mass and momentum balances applied to each channel yield the system of governing ordinary differential equations for transport in each process. Eqs. (1)–(3) describe changes in crossflow velocity $u(x)$, solute concentration $c(x)$, and pressure $p(x)$, with position $x$ (module length) in the dilute and concentrated channels, *viz.*,

$$\frac{du}{dx} = \pm\frac{2J_w}{h} \tag{1}$$

$$\frac{d(uc)}{dx} = \pm\frac{2J_s}{h} \tag{2}$$

$$\frac{dp}{dx} = -\frac{\lambda\rho u^2}{2d_h} \tag{3}$$

where $h$ is the PRO or RED module channel height, $\rho$ is the density of water, $d_h$ is the hydraulic diameter of the channel, $J_w$ is the water flux across the membrane, $J_s$ is the salt flux, and $\lambda$ is the friction factor coefficient. An exhaustive study was conducted in order to identify useful friction factor correlations in the literature. Many correlations have been developed for different flow geometries and Reynolds numbers. Here we apply a friction factor correlation which is relevant to the range of conditions modeled in this study [17]. The friction factor coefficients used in determining the hydraulic losses within each channel were calculated through

$$\lambda = \omega_1 - \frac{\omega_2}{Re^{\omega_3}} \tag{4}$$

where $\omega_1$, $\omega_2$, and $\omega_3$ are fitting parameters obtained from computational fluid dynamics [17]. For the case of circular spacers with a diameter half the channel height and 4.5 mm filament spacing, the values of these parameters are $\omega_1 = 0.42$, $\omega_2 = 189.29$, and $\omega_3 = 1$. Please see the Supporting information for more details on our approach to the friction factor correlation.

A graphical representation of a single PRO or RED membrane "cell" is shown in Fig. 1. Note that in Eqs. (1) and (2), negative and positive signs signify mass loss and gain, respectively, occurring in the dilute and concentrated channel. Furthermore, we define the dilution ratio, i.e., the ratio of dilute to concentrated channel flow rates, as

$$d_r = \frac{q_d}{q_c}. \tag{5}$$

The dilution ratio has a fundamental impact on the energy efficiency achieved during mixing, as well as the total power extracted. It is distinctly a feature of large-scale implementation; such effects have not received attention in the laboratory-scale literature.

### 2.1. Water and salt fluxes

#### 2.1.1. PRO

Water flux in PRO is a function of the bulk solute concentrations (and hence, the osmotic pressure), salt diffusivity $D$, external mass transfer coefficient $k_c$, universal gas constant $R$, temperature $T$, and membrane permeability to water, $A$, and salt, $B$ [5]. In order to account for the impact of non-ideality in the osmotic pressure, a correction factor must be applied. The actual osmotic pressure ($\pi_{actual}$) and the ideal osmotic pressure ($\pi_{ideal}$) can be related through the concentration-dependent osmotic coefficient ($\phi$),

$$\phi = \frac{\pi_{actual}}{\pi_{ideal}} = \frac{(RT/\overline{V})\ln a_w}{2RTc} \tag{6}$$

where the numerator is the actual osmotic pressure and considers the activity of water ($a_w$), and thus non-ideality, and the denominator is the idealized van't Hoff approximation for osmotic

pressure. Here, $\overline{V}$ is the molar volume of water. Using published reference data [18,19], it is possible to construct a numerical correlation to determine the osmotic coefficient of water at a given concentration (i.e., $\phi = f(c)$). Please see the Supporting information for further details on the numerical correlation applied in this study. The membrane interface concentrations (subscript $m$) for the dilute and concentrated feed (subscripts $d$ and $c$, respectively) are defined as [20]

$$c_{c,m} = c_{c,b}\exp\left(\frac{-J_w}{k_c}\right) - \frac{B}{J_w}(c_{c,m} - c_{d,m})\left[1 - \exp\left(\frac{-J_w}{k_c}\right)\right] \tag{7}$$

and

$$c_{d,m} = c_{d,b}\exp\left(\frac{J_w S}{D}\right) + \frac{B}{J_w}(c_{c,m} - c_{d,m})\left[\exp\left(\frac{J_w S}{D}\right) - 1\right] \tag{8}$$

where

$$c_{c,m} - c_{d,m} = \frac{c_{c,b}\exp(-J_w/k_c) - c_{d,b}\exp(J_w S/D)}{1 + \frac{B}{J_w}[\exp(J_w S/D) - \exp(-J_w/k_c)]}. \tag{9}$$

Here, $S$ is the structure factor, dependent on the porosity, tortuosity and thickness of the membrane support layer, which dictates the severity of salt accumulation within it (internal concentration polarization). We apply $\pi_{actual} = \phi 2RTc$ (from Eq. (6)) to calculate the actual osmotic pressure difference between the two feeds, with $c = c_{d,m}$ and $c = c_{c,m}$ for $\pi_{actual,d}$ and $\pi_{actual,c}$, respectively. Here, the value of the osmotic coefficient is determined from the constructed correlation and is calculated for both the concentrated and dilute solution membrane interface concentrations ($\phi_{c,\ m}$, and $\phi_{d,\ m}$, respectively). The flux can then be determined through

$$J_w = A(\Delta\pi_{actual} - \Delta p), \tag{10}$$

where $\Delta\pi_{actual} = \pi_{actual,\ c} - \pi_{actual,\ d}$ and $\Delta p = p_c - p_d$ are the applied pressure differences between the two feeds $A$.

The salt flux (or "salt leakage") is assumed to be purely diffusive and, accounting for concentration polarization effects, is given by [5]

$$J_s = B\left[\frac{c_c exp(-J_w/k_c) - c_d exp(J_w S/D)}{1 + \frac{B}{J_w}(exp(J_w S/D) - exp(-J_w/k_c))}\right]. \tag{11}$$

#### 2.1.2. RED

The RED salt flux is composed of both Coulombic ($J_{coul}$) and co-ion transport ($J_{cit}$) components, i.e., $J_s = J_{coul} + J_{cit}$ [10]. The Coulombic flux component can be described by

$$J_{coul} = \frac{\Delta V_{mem} - \Delta V_{load}}{F r_{stack}}, \tag{12}$$

where $F$ is the Faraday constant, $\Delta V_{load}$ is the voltage drop across the external load, $r_{stack}$ is the internal stack resistance incorporating average ion exchange membrane resistance ($r_{mem}$), as well as dilute ($r_d$), and concentrated ($r_c$) channel resistances. The potential difference across the membrane, $\Delta V_{mem}$, is defined as

$$\Delta V_{mem} = \frac{\alpha 2RT}{F}\ln\frac{\gamma_{c,m} c_{c,m}}{\gamma_{d,m} c_{d,m}}, \tag{13}$$

where $\alpha$ is the average permselectivity, and $\gamma_{c,m}$ and $\gamma_{d,m}$ are the sodium chloride activity coefficients for the concentrated and dilute solutions, respectively, as a function of membrane concentration [10]. As with the osmotic coefficient for PRO, we constructed a numerical correlation relating sodium chloride activity to concentration using data from the literature [18,19]. Details for the numerical correlation are included in the Supporting information. The subscript $m$ refers to the membrane interface concentration and is related to the bulk concentration ($c_b$) via

$$c_m = c_b \pm \frac{J_{coul}}{k}, \tag{14}$$

which accounts for ion accumulation (depletion) at the membrane surface in the dilute (concentrated) channel. Since $J_{coul} \gg J_{cit}$, we only consider the effect of the Coulombic flux in concentration polarization. The co-ion flux component is defined as

$$J_{cit} = \frac{D_{mem}}{\delta_{mem}}(c_{c,m} - c_{d,m}), \tag{15}$$

where the salt diffusion coefficient within the membrane is denoted by $D_{mem}$ and the thickness of the membrane by $\delta_{mem}$ [10]. We assume negligible net osmotic flux through the ion exchange membranes due to the competing contributions of osmosis and electro-osmosis [21].

### 2.2. External mass transfer

The feed side external mass transfer coefficients were determined using correlations for a rectangular, spacer filled channel. As with the friction factor coefficient detailed in the earlier section, an exhaustive review of the available literature was conducted in order to identify the most useful correlations. Please see the Supporting information for more details on our approach to the mass transfer coefficient. The chosen correlations were specifically derived for RO but here we apply them for both PRO and RED. The

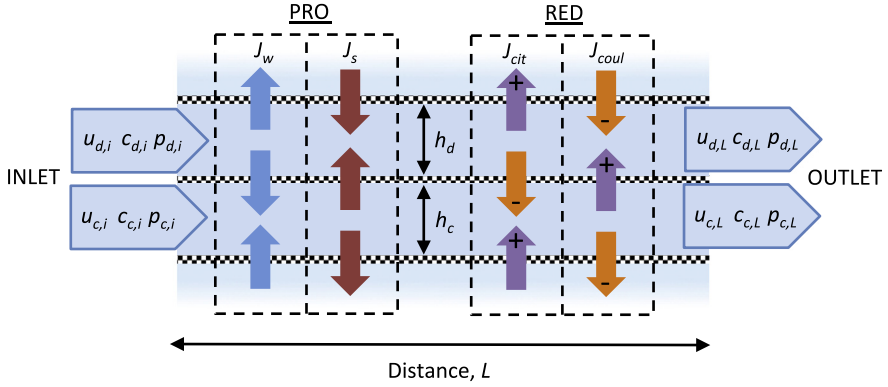


**Fig. 1.** Graphical representation of a unit "cell" for PRO and RED. Note that initial flow conditions are denoted by the subscript $i$, while conditions at a given module length $L$ are represented by subscript $L$. PRO involves water flux ($J_w$) and salt flux ($J_s$), while RED consists of a co-ion transport flux ($J_{cit}$) and Coulombic flux ($J_{coul}$) for positive and negative ions.

mass transfer coefficient, $k_c$, can be calculated via [17]

$$k_c = 0.46(Re\,Sc)^{0.36}\frac{D}{d_h} \tag{16}$$

where $Re = ud_h\rho/\mu$ is the Reynolds number (i.e., the ratio of inertial-to-viscous forces in a flow), where $\mu$ is the dynamic viscosity of the solution, and $Sc = \mu/\rho D$ is the Schmidt number (i.e., the ratio of typical time scales for diffusive momentum and mass transport).

### 2.3. Applied pressure and load voltage

In order to produce power in real systems, a hydraulic pressure (for PRO) or load voltage/resistance (for RED) must be applied. In PRO, the applied pressure corresponds to some multiple, represented here as $1/f$ of the total available osmotic pressure difference ($\Delta\pi$) between the dilute and concentrated feeds. Here, $f$ is termed as the load factor, where the value of $f$ must be greater than unity for the process to operate in PRO mode. The initial osmotic pressure difference is given by $\Delta\pi_i = \phi_{c,b}2RTc_{c,b} - \phi_{d,b}2RTc_{d,b}$ using the bulk (and not the membrane interface) concentration difference between the dilute and concentration feeds. Bulk concentrations are used since the membrane interface concentrations are a function of the water flux, and therefore, the membrane properties and geometrical proportions of the channel. By using the bulk concentration, the applied pressure is a function of the solution properties alone. Likewise, in RED, the load voltage is represented as $1/f$, taken here relative to the initial potential difference $\Delta E$, where the open circuit voltage is given by $\Delta E_i = (2RT/F)\ln(\gamma_{c,b}c_{c,b}/\gamma_{d,b}c_{d,b})$. As with PRO, here bulk concentrations are used instead of membrane interface concentrations. For both processes, ignoring viscous dissipation, maximum power density is achieved when the applied pressure difference or load voltage is exactly half of the available osmotic pressure or open circuit voltage, i.e., $\Delta p = \Delta\pi/2$ and $\Delta V = \Delta E/2$, where $\Delta p$ is the difference in hydraulic pressure between the feeds and $\Delta V$ is the applied load voltage [1]. In a large-scale system where pressure and concentration vary with length, the applied pressure must be adjusted to account for these changing conditions. Hence, for PRO we define the initial dilute feed pressure as the minimum pressure necessary to overcome hydraulic losses in the dilute channel and define the initial concentrated feed pressure (which is far in excess of the dilute feed pressure) to equal

$$p_{c,i} = \frac{\Delta\pi_i}{f} + p_{d,i} - p_{d,L}, \tag{17}$$

where $\Delta\pi_i$ is the initial osmotic pressure difference between the concentrated and dilute solutions, $p_{d,i}$ and $p_{d,L}$ are the initial dilute feed applied pressure and the applied pressure of the dilute feed at some distance $L$. As noted earlier, for maximum power density in an idealized, constant pressure system, $f = 2$; however, as will be shown, this condition does not necessarily correspond to maximum power density or energy efficiency in a full-scale system.

For RED, the applied load is not linked with dissipation due to module length as in PRO, and is defined as

$$\Delta V_{load} = \frac{\Delta E_i}{f}, \tag{18}$$

where $\Delta E_i$ is the initial potential difference between the concentrated and dilute channels.

### 2.4. Net power and power density

In general, the maximum reversible power $P_{rev}$ that can be extracted from mixing a dilute feed and a concentrated feed can be written as

$$P_{rev} = 2RT\left(q_{d,i}c_{d,i}\ln\frac{c_{d,i}}{c_{eq}} + q_{c,i}c_{c,i}\ln\frac{c_{c,i}}{c_{eq}}\right), \tag{19}$$

where $c_{eq}$ is the equilibrium concentration at complete mixing

$$c_{eq} = \frac{c_{c,i} + d_r c_{d,i}}{1 + d_r}. \tag{20}$$

In the PRO configuration envisioned here, only the permeate flow is passed through the hydroturbine while the initial flow is passed through a hydraulic energy recovery (HER) device where energy is exchanged with the concentrated feed prior to flow through a high pressure pump. The net power generated for a module of a given length, $L$, can be determined by subtracting the contribution of the pumping energy demand for the dilute and concentrated feeds from the power generated by the hydroturbine, i.e., $P_{net} = P_{ht} - P_{p,}$ where

$$P_{ht} = \eta_{ht}bh_c p_{c,L}\int_0^L J_w\,dx \tag{21}$$

and

$$P_p = \frac{q_{c,i}}{\eta_p}(p_{c,i} - \eta_{her}p_{c,L}) + \frac{q_{d,i}}{\eta_p}(p_{d,i} - p_{d,L}), \tag{22}$$

where $\eta_{ht,}$ $\eta_p$ and $\eta_{her}$ denote the efficiencies of the hydro-turbine, pump, and hydraulic energy recovery device, respectively, and $b$ is the width (hereafter taken as unity). The first term on the right hand side of Eq. (22) is the power necessary to pump the concentrated feed, where the energy consumption is reduced due to the contribution of the HER device.

In RED the net power is calculated by determining the power dissipated by the external load, and subtracting the pumping power demand for the concentrated and dilute feeds, i.e., $P_{net} = P_{load} - P_p$, where

$$P_{load} = bF\Delta V_{load}\int_0^L J_{coul}\,dx \tag{23}$$

and

$$P_p = \frac{q_{c,i}(p_{c,i} - p_{c,L}) - q_{d,i}(p_{d,i} - p_{d,L})}{\eta_p}. \tag{24}$$

The system-level power density, for both PRO and RED, can be calculated by dividing the net power by the total membrane area

$$P_d = \frac{P_{net}}{2bL}, \tag{25}$$

where division is by 2 accounts for the fact that there are two membranes in a single unit cell. Power density is the quantity most frequently used in the literature for comparing RED vs. PRO process performance. Here we define the total process efficiency as the total generated power (or work) divided by the theoretical power (or work) available with completely reversible mixing

$$\eta = \frac{P_{net}}{P_{rev}}. \tag{26}$$

Note that this value corresponds to the fraction of the reversible work, and not to the available work, that is recovered through mixing [8]. Since the reversible (but not the available) work is the same for PRO and RED, this approach maintains continuity in the analysis.

### 2.5. Solution methodology

The non-linear system of ordinary differential equations [Eqs. (1)–(3)] and algebraic constraints [Eqs. (10)–(12) and (15)] outlined above for each process were solved using the freely available

APMonitor modeling environment [22]. For the present study, parameters representative of state-of-the-art commercially available membranes were applied in the process modeling, namely, the Oasys thin film composite (TFC) forward osmosis (FO) membrane was used for PRO, while the Neosepta AMX-CMX and Fumasep FKD-FAD anion exchange–cation exchange membrane pair was used for RED. The dilute feed (treated wastewater or river water) concentration is taken as 17 mol/m$^3$ NaCl while the concentration feed (seawater) concentration is taken as 513 mol/m$^3$. Table 1 lists the values of different process parameters used in the simulations. Unless otherwise stated, crossflow velocities for both RED and PRO are taken as 0.02 m/s for all process simulations. A brief comparison of our modeling results with published experimental data from a 1 m long PRO module [23] is included in the Supporting information. Unfortunately, we have only been able to conduct this analysis for PRO, since we could not find any comparable experimental data for RED. Calculations illustrate that the water flux from our model is in very reasonable agreement with water flux reported from the module size study, especially at lower applied pressures. We note that discrepancies may inherently present themselves due to uncertainty in the parameters used in the experimental study, as well as in the specific module geometry.

Note that, as the model predicts that mixing will proceed until the driving force is infinitesimally small, some threshold must be set in order to determine the relative location of equilibrium. Therefore, $J_w \approx 0$ and $J_{coul} \approx 0$ actually correspond to prescribed values where $J_w = 10^{-9}$ m s$^{-1}$ and $J_{coul} = 10^{-10}$ mol m$^{-2}$ s$^{-1}$. These values correspond to approximately 0.1% of the initial flux for PRO and RED when operating under the conditions listed in Table 1 and at crossflow velocity $u = 0.02$ m/s and load factor $f = 2$.

## 3. Results and discussion

### 3.1. Properly calculating power density

The commonly accepted method to assess the power density in PRO is to multiply the experimentally determined flux (i.e., average flux, $\bar{J}_w$) by the (constant) concentrated feed applied pressure, i.e., $P_d = \bar{J}_w p_{c,i}$. However, this method grossly overestimates the actual power density achievable in a PRO module since it ignores the contribution of hydraulic losses and machine (hydro-turbine, pump, and HER device) inefficiencies. In Fig. 2, the power density has been calculated using both the commonly published method and through the method discussed in Eq. (25), which incorporates losses. It is clear from the results that there is a significant impact on the power density from incorporating these losses. Although it is not surprising that hydraulic losses reduce the achievable power density, there is also an unforeseen impact due to machine inefficiency. In fact, when operating at a relatively low crossflow velocity (and correspondingly low hydraulic losses), the efficiency of the hydraulic energy recovery device becomes the primary contributor to reduced power density. This effect shifts the power density to negative values at short module length. The reduced power density can be explained due to the high pressures needed on the concentrated solution side in order to operate near the optimum power density. For example, although current HER devices can operate at $\eta_{her} > 0.95$, the energy lost when transferring pressure (energy) to the PRO concentrated feed from the PRO brine, i.e., $(1-\eta_{her})p_{c,L}q_{c,i}$, is still very significant when $p_{c,L}$ is large. Further increasing the already high value of $\eta_{her}$ may not be technically feasible. Note that the size of most laboratory-scale PRO membranes is in the order of centimeters rather than meters, and therefore only power density near the maximum value is reported. Due to the efficiency considerations shown, a membrane module of this length will in fact have low or negative power density depending on the efficiency of the HER device.

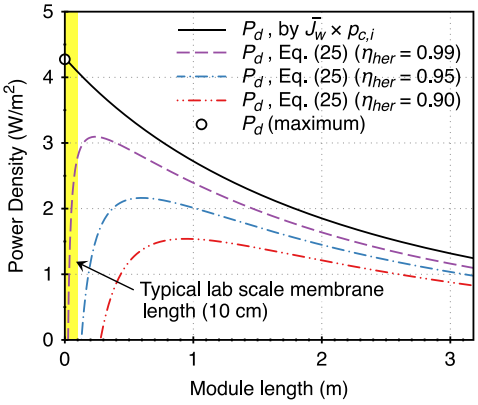


**Fig. 2.** Change in PRO power density with module length, using different calculation methods. Note that the commonly accepted method for extrapolating the power density from experimental data (black line) results in much higher power density than when losses and inefficiencies are considered. The yellow shaded area represents the region where most power density measurements are observed in the laboratory due to small-scale experimental design. All calculations for PRO were made with $f = 2$, and $u = 0.02$ for both channels. (For interpretation of the references to color in this figure legend, the reader is referred to the web version of this article.)

Since RED does not require a significant applied pressure in order to extract energy, RED does not employ an HER device. Therefore, the change in the power density profile at short module length due to HER device inefficiency is not observed for RED. This distinction is a particularly important difference between PRO and RED. For RED, power density is maximized at infinitely short module length (see later sections) while for PRO there exists a maximum power density when module length is appreciably greater than zero. Of course, since both the actual value of maximum power density and the associated membrane/module cost are different for each process, this does not imply that either process is inherently superior. A full scale cost analysis is necessary in order to determine for which process the dollar invested per unit energy produced can be maximized.

### 3.2. Change in applied pressure and load

In order to provide a useful indication of the relative process performance at different operating conditions, the developed model has been used to calculate both power density and efficiency. Fig. 3 shows how these metrics change with system length when operating at different load factors. Power density (which is obtained from the total, system-integrated power divided by the membrane area) indicates the system-average productivity of the total available membrane area. In a system that does not account for losses, power density

**Table 1**
Overview of process parameters.

| Parameter | Value | Reference |
|---|---|---|
| *PRO*: | | |
| Membrane hydraulic permeability, $A$ | $9.56 \times 10^{-12}$ m/(s Pa) | [27] |
| Membrane salt permeability, $B$ | $1.31 \times 10^{-7}$ m/s | [27] |
| Membrane structure factor, $S$ | 434 μm | [27] |
| Channel height, $h$ | 700 μm | |
| *RED*: | | |
| Average membrane resistance, $r_{mem}$ | $2.63 \times 10^{-4}$ Ω m$^2$ | [1] |
| Average permselectivity, $\alpha$ | 0.949 | [1] |
| Channel height, $h$ | 200 μm | |
| *General*: | | |
| Pump efficiency, $\eta_p$ | 0.89 | [25] |
| Hydroturbine efficiency, $\eta_{ht}$ | 0.90 | [25] |
| HER device efficiency, $\eta_{her}$ | 0.95 | [8] |
| Solution molar conductivity | 0.01287 (S m$^2$)/mol | [11] |
| Temperature, $T$ | 293 K | |

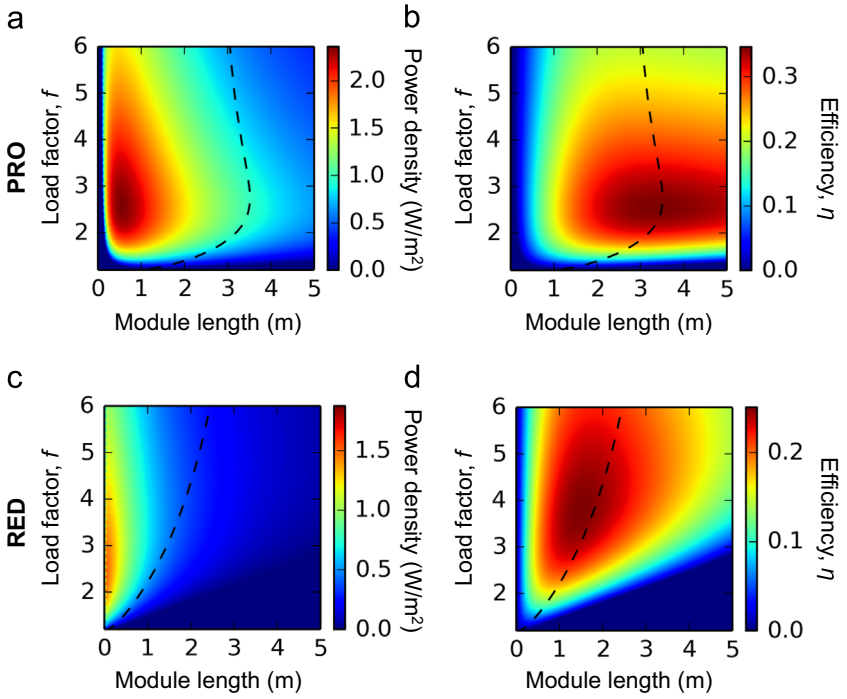


**Fig. 3.** Change in power density and efficiency for PRO (a,b) and RED (c,d), with variation in load factor and module length. The dashed black line on all plots corresponds to the module length at which mixing approaches equilibrium (i.e., $J_w \approx 0$ for PRO and $J_{coul} \approx 0$ for RED) for the given set of operational conditions. All simulations were conducted at a crossflow velocity of $u = 0.02$ m/s for both the concentrated and dilute feed channels.

is maximized for an infinitesimally short system length (where no dilution occurs), while efficiency is maximized at equilibrium (complete mixing). However, especially for the case of PRO (Fig. 3a), power density is not maximized until approximately 0.5 m of system length. Again, this shift in maximum power density is due to the inclusion of pump, hydro-turbine, and pressure exchanger inefficiencies. These require that a finite amount of power be produced by the system to overcome inherent losses. In our calculations, system-averaged power densities approach 2.0 W/m$^2$ for RED and 2.5 W/m$^2$ for PRO.

While power density and efficiency appear to be maximized at approximately the same load factor for PRO, this does not occur at $f = 2$, as predicted theoretically [1,3,5]. Rather, the maximum occurs at $f \approx 2.5$, meaning that a substantially lower applied pressure is necessary compared to the ideal case, due to process inefficiencies and dilution. In RED, efficiency is highest at $f \approx 3.8$ while power density is maximized at $f \approx 2.1$, again suggesting there is a significant gap between the real and idealized cases. The dashed black lines shown on the plots in Fig. 3 represent the module length corresponding to equilibrium for each applied load factor. For PRO, the maximum value for module length lies at the load factor maximizing efficiency and power density.

### 3.3. Change in crossflow velocity

The crossflow velocity is one operational parameter that appears to fundamentally impact process performance. Velocity variation has been modeled in two ways, (1) the dilution ratio has been set to unity and the concentrated and dilute feed velocities varied together over a selected range, and (2) the sum of the concentrated and dilute feed velocities has been set constant at 0.04 m/s with the dilution ratio varied. This does not mean that the same flow rates apply for PRO and RED at a given dilution ratio. Rather, crossflow velocities are the same for PRO and RED, but due to the different channel heights for each process the flow rates are necessarily different. This approach was taken in order to capture comparable power densities for both processes. For example, applying a relatively high flow rate for PRO will produce a relatively higher power density, but applying the same flow rate for RED may result in unacceptably high viscous dissipation in the flow channels. This is a consequence of the two processes possessing fundamentally different engineering constraints. Here the system represents a simple two channel "cell" as detailed in Fig. 1. Fig. 4 depicts the change in power density and efficiency, for PRO and RED with change in velocity at constant dilution ratio. For PRO (Fig. 4a,b), it is clear that the power density and efficiency diminish significantly above 0.1 m/s. This result is particularly interesting considering the agreed upon "standard method" for testing FO and PRO membranes is at a crossflow velocity of 0.25 m/s [24]; such a high crossflow velocity appears impractical in large-scale implementation of PRO. A similar change in crossflow velocity for RED results in an even narrower region of preferred operation (Fig. 4c,d). The smaller channel height in RED increases the impacts of hydraulic pressure losses on the average power density and efficiency.

### 3.4. Change in dilution ratio

Varying the dilution ratio at a constant total crossflow velocity ($u = 0.04$ m/s) indicates that increasing the dilution ratio results in higher efficiency for RED, but lower efficiency for PRO (Fig. 5). It is also clear from the data that, for PRO, operating near a dilution ratio of unity leads to maximum system length (i.e., more membrane is necessary to achieve thermodynamic equilibrium). For RED, membrane area is maximized at $2 < d_r < 3$. The results incorporate the thermodynamic effect of changing mixing volumes as well as external mass transfer and hydraulic pressure loss effects.

### 3.5. Maximum values

As has been demonstrated above, the process model can be used to determine how important performance metrics change under different operating conditions. From Figs. 3 to 5, it is clear that the values for power density and efficiency change with dilution ratio, load factor, and crossflow velocity. However, in the preceding set of calculations, each of these operating parameters was varied individually with

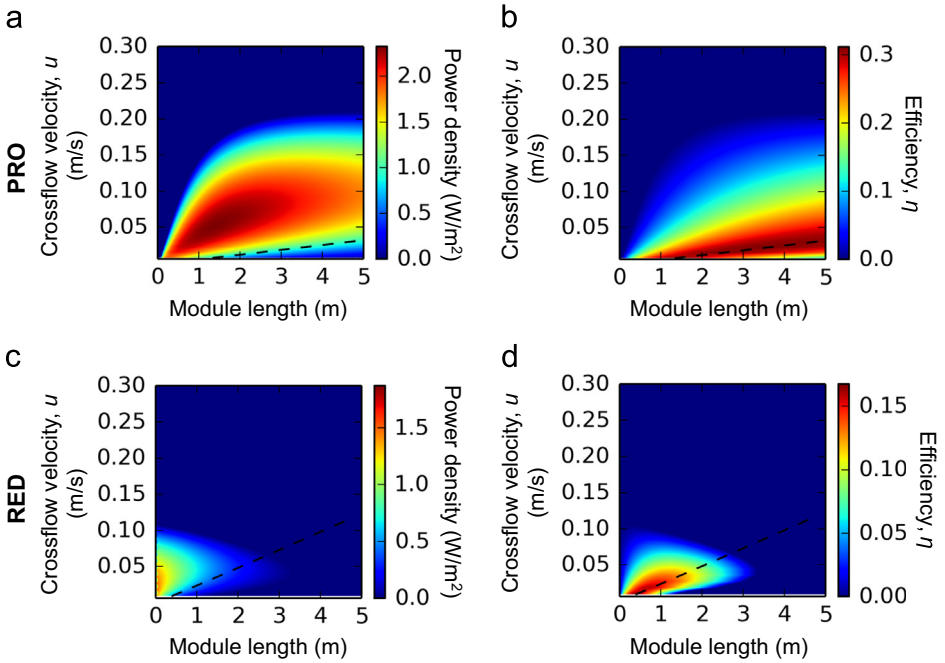


**Fig. 4.** Change in power density and efficiency for PRO (a,b) and RED (c,d), with variation in crossflow velocity and module length. The dashed black line on all plots corresponds to the module length at which mixing approaches equilibrium (i.e., $J_w \approx 0$ for PRO and $J_{coul} \approx 0$ for RED) for the given set of operational conditions. All calculations for PRO and RED were made with $f=2$.

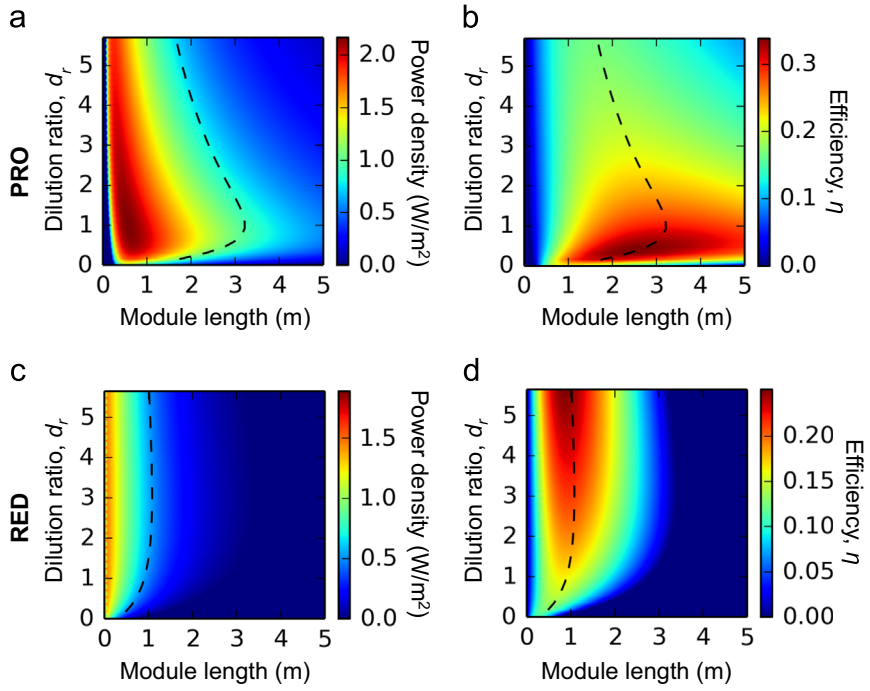


**Fig. 5.** Change in power density and efficiency for PRO (a,b) and RED (c,d), with variation in dilution ratio and module length. The dashed black line on all plots corresponds to the module length at which mixing approaches equilibrium (i.e., $J_w \approx 0$ for PRO and $J_{coul} \approx 0$ for RED) for the given set of operational conditions. Calculations were made with a total crossflow velocity $u=0.04$ m/s, with dilution ratio variation achieved by taking different fractions of the total velocity. All calculations for PRO and RED were made with $f=2$.

respect to module length. It is useful to identify how the maximum values for three performance metrics – power ($P_{net}$), power density ($P_d$), and efficiency ($\eta$) – change as operating conditions are changed simultaneously rather than one at a time. Here, dilution ratio and load factor have been chosen as the variable operating conditions. In order to conduct the analysis, the maximum value for each performance metric was evaluated for different system lengths, and the largest value was plotted against the relevant load factor. Note that, as the load factor necessarily impacts the driving force and equilibrium in each case, module length is not constant across all scenarios, and is rather a model output, giving a value of the system size at which a maximum is achieved for either the total power, power density or efficiency. Fig. 6 shows how changes in load factor impact the maximum energy efficiency, power, and power density for several dilution ratios ($d_r=0.25$, 1, 4) when all process losses are incorporated. Dilution ratio variation has been achieved using the method described earlier.

While all dilution ratios show roughly similar maximum power density values, the power output and efficiency vary significantly

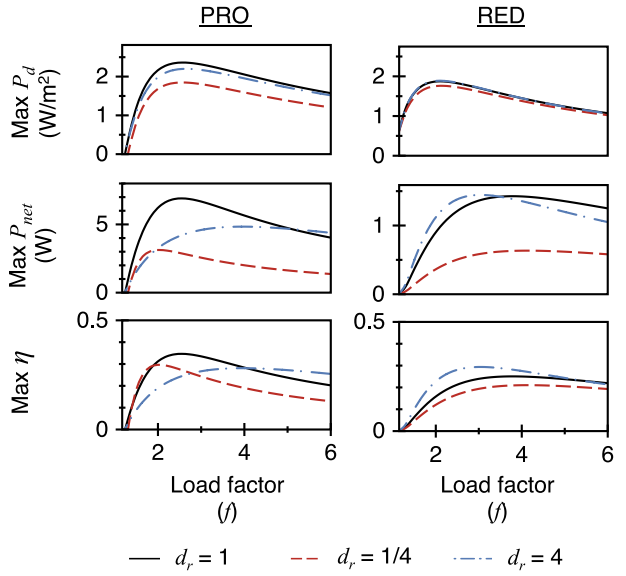


**Fig. 6.** Change in maximum power density ($P_d$), maximum power ($P_{net}$), and maximum efficiency ($\eta$) for PRO (left column) and RED (right column) as the load factor ($f$) is varied at different dilution ratios.

with dilution ratio. Thus, reporting a maximum power density value alone is an incomplete measure for judging the performance of an SGP process since these maximum power densities may correspond to different system sizes. Furthermore, the data show that higher energy efficiency does not necessarily correspond to higher overall power output. For example, in RED, operating at $d_r=4$ is more efficient than operating at $d_r=1$, yet both scenarios produce roughly the same overall power output. A similar behaviour can be observed for PRO. In an ideal case, the efficiency will vary only by changing the ratio of the feed flow rates and not the magnitude of the flow rates. Accounting for losses introduces some impact of the actual flow rate magnitude on energy efficiency due to viscous losses and mass transfer limitations (external concentration polarization). In either case, the power produced is of course proportional to the mixed volumes. For example, if 10 $m^3$ of river water were mixed with 40 $m^3$ of seawater, one would naturally expect greater overall power output than from mixing 0.10 $m^3$ of river water with 0.10 $m^3$ of seawater, despite the higher overall efficiency in the latter case.

Over the range of flow rates modeled, RED displays higher maximum efficiency with increasing dilution ratio. A larger relative dilute feed flow rate maintains low concentrations and thus ensures a more sustained potential difference across the membrane. PRO, on the other hand, does not exhibit a clear trend over the dilution ratios modeled. In theory, a relatively larger concentrated solution flow rate results in greater sustained osmotic pressure difference between the two solutions, since each molecule of water crossing the membrane has relatively lessened dilutive effect. However, in a non-ideal system, increasing the concentrated feed flow rate results in greater viscous dissipation in the feed channel, decreasing the overall energy efficiency.

Recall that, in an ideal case, power density is maximized at $f=2$. As already established earlier (see Fig. 3), power density and efficiency are not maximized at this value. However, while maximum power density peaks at the same load factor for all modeled dilution ratios, this is not the case for maximum efficiency or maximum power (Fig. 6). Varying the dilution ratio necessarily changes the preferred load factor. These effects are shown to be of great importance and so must be considered when determining the optimum operating regime.

As noted earlier, maximum membrane area per "cell" (i.e., the system length necessary to achieve $J_w \approx 0$ or $J_{coul} \approx 0$, multiplied by unit width and a factor of two to account for two membranes), necessarily changes with varying inlet conditions. To determine the maximum membrane area, one cannot simply divide the total maximum power by the maximum power density shown in Fig. 6, since each of these metrics is maximized at a different system size. Still, it is instructive to identify how maximum area changes with dilution ratio and we can extract this value from the process model. From Fig. 7, it is clear that maximum membrane area scales differently with varying dilution ratio for PRO and RED. As noted earlier, these results are per "cell," at the same cross flow velocities for PRO and RED, and not at equal flow rate. For RED, membrane area appears to increase with increasing load factor, irrespective of the actual dilution ratio. On the other hand, for PRO, maximum membrane area appears to peak at lower load factors for some dilution ratios. This behavior is a consequence of the way the driving force ($\Delta\pi$ or $\Delta V_{mem}$) and retarding force ($\Delta p$ or $\Delta V_{load}$) impact the flux equations for each process.

### 3.6. Cost considerations

Ultimately, the cost to produce a kilowatt-hour of energy and the installed cost (per kW) are the most important metrics in evaluating energy production, and for designing full-scale membrane area requirements (here represented by module length). It is also the most practical basis for comparison between RED and PRO processes and, ultimately, between SGP and other forms of electricity generation. Since it would not be economically viable to seek complete mixing (i.e., equilibrium), the most cost-effective system lengths will lie somewhere between the maximum power density and efficiency.

For an SGP process, total membrane module cost will scale with membrane area. However, assuming constant crossflow velocity, there is a tradeoff between the cost associated with pump flow rate requirement (higher for cells in parallel) and pump pressure requirement (higher for cells in series due to higher pressure drop). With the input of cost correlations for each of the system components (pumps, membrane modules, HER device, etc.), it is possible to use the process model to optimize the cost relative to the system power output. That is, one can determine the location of maximum cost-effectiveness (i.e., the effective length or number of cells in series) depending on the relative capital costs of different plant components. Operating costs, which may scale differently than capital costs, can also be considered in the overall cost optimization. For example, pump capital cost could outweigh membrane capital cost in very short modules, but the operating cost associated with membrane cleaning could be more significant than pump maintenance. Of course, the accuracy of such an analysis will depend on the quality of the cost correlations used for the various plant components.

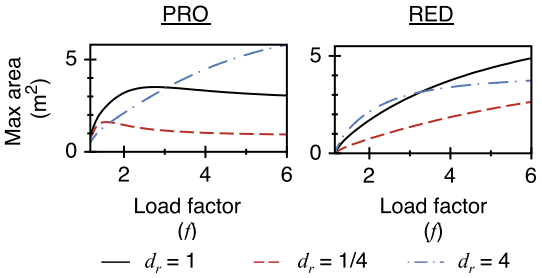


**Fig. 7.** Change in maximum membrane area for one "cell" (i.e., the system length necessary to achieve $J_w \approx 0$ or $J_{coul} \approx 0$, multiplied by unit width and a factor of two to account for two membranes), for PRO (left column) and RED (right column) as the load factor ($f$) is varied at different dilution ratios.

While it is possible to use empirical cost correlations for RO and ED to estimate costs for PRO and RED, respectively, the classical models do not realistically predict optimized full-scale performance. Loeb used a different method for his analyses of PRO feasibility [25,26]. However, Loeb did not apply a full-scale process model to determine how power density changes with system size, and instead extrapolated the cost for PRO based on the cost per cubic meter of permeate volume produced by RO. Our work suggests that such an approach may be unsubstantiated, due to inherent differences between RO and PRO. Future work to determine PRO or RED cost should rely on appropriate full-scale process model results (such as those presented here) as well as updated empirical correlations for plant component capital cost, operating cost, construction cost, and other contributing costs.

## 4. Conclusions

Newly developed large-scale performance models of PRO and RED processes enable practical simulations of power density, production and efficiency for SGP. The results demonstrate the following:

1) HER device efficiency can significantly impact the power density and energy efficiency profiles for PRO. An important future research area is the refinement and improvement of HER devices for the operating pressures likely to be encountered in PRO.
2) The impact of cross-flow velocity is clear. In particular, PRO studies commonly employ velocities that (according the results of this study) are likely to consume significant power output at full-scale.
3) Load pressures and voltages typically identified as the preferred operating regimes for PRO and RED are shown here to be non-ideal. Therefore, full-scale implementation of either process should not rely on predictions from simpler models.
4) The highest energy efficiency does not necessarily occur at thermodynamic equilibrium for both processes due to viscous dissipation. Furthermore, energy efficiency appears to be maximum at lower dilution ratios for PRO and higher dilution ratios for RED. Depending on the relative availability of the dilute or concentrated feed, this could imply a preference for a particular process.
5) Since membrane area varies significantly with dilution ratio, maximum power density is an inadequate metric for comparing a process with different operating conditions.

The data presented here demonstrate that the power densities achievable from PRO and RED are well below those predicted by extrapolating lab-scale measurements with idealized models. Since the modeled scenario corresponds to ocean water-river water mixing, future work should focus on applications with significantly different salinity gradients which may require unique operating conditions to optimize performance.

## Acknowledgments

We are grateful for financial support for this research provided by the Clean Energy for Green Industry (CGI) NSF IGERT at UCLA. G.Z.R was supported by a Marie-Curie IOF grant no. 275911 under the FP7 program of the European Research Council.

## Appendix A. Supporting information

Supplementary data associated with this article can be found in the online version at http://dx.doi.org/10.1016/j.memsci.2014.10.023.

## Nomenclature

| | |
|---|---|
| $A$ | water permeability coefficient, m $Pa^{-1}$ $s^{-1}$ |
| $B$ | salt permeability coefficient, m $s^{-1}$ |
| $b$ | module width, m |
| $c$ | concentration, mol $m^{-3}$ |
| $c_{eq}$ | equilibrium concentration, mol $m^{-3}$ |
| $D$ | solute diffusion coefficient in water, $m^2$ $s^{-1}$ |
| $d_h$ | hydraulic diameter, m |
| $d_r$ | dilution ratio |
| $D_{mem}$ | solute diffusion coefficient in membrane, $m^2$ $s^{-1}$ |
| $\Delta E$ | open circuit voltage, V |
| $F$ | Faraday constant, C $mol^{-1}$ |
| $f$ | load factor |
| $h$ | channel height, m |
| $J_{cit}$ | co-ion flux, mol $m^{-2}$ $s^{-1}$ |
| $J_{coul}$ | Coulombic flux, mol $m^{-2}$ $s^{-1}$ |
| $J_s$ | salt flux, mol $m^{-2}$ $s^{-1}$ |
| $J_w$ | water flux, m $s^{-1}$ |
| $k_c$ | external mass transfer coefficient, m $s^{-1}$ |
| $L$ | module length, m |
| $p$ | pressure, Pa |
| $P_d$ | power density, W $m^{-2}$ |
| $P_{ht}$ | power generated through hydro-turbine, W |
| $P_{load}$ | power generated through external load, W |
| $P_{net}$ | net power, W |
| $P_p$ | pump demand, W |
| $P_{rev}$ | power from reversible mixing, W |
| $q$ | volumetric flow rate, $m^3$ s |
| $R$ | universal gas constant, J $mol^{-1}$ $K^{-1}$ |
| $Re$ | Reynolds number |
| $r$ | resistance, $\Omega$ $m^2$ |
| $r_{mem}$ | membrane resistance, $\Omega$ $m^2$ |
| $r_{stack}$ | stack resistance, $\Omega$ $m^2$ |
| $S$ | structure parameter, m |
| Sc | Schmidt number |
| Sh | Sherwood number |
| $T$ | absolute temperature, K |
| $u$ | Crossflow velocity, m $s^{-1}$ |
| $\Delta V_{mem}$ | voltage drop across membrane, V |
| $\Delta V_{load}$ | voltage drop across external load, V |
| $x$ | distance, m |

*Greek letters*

| | |
|---|---|
| $\alpha$ | permselectivity |
| $\gamma$ | salt activity coefficient |
| $\delta_{mem}$ | membrane thickness, m |
| $\eta$ | efficiency |
| $\eta_{her}$ | HER-device efficiency |
| $\eta_{ht}$ | hydroturbine efficiency |
| $\eta_p$ | pump efficiency |
| $\lambda$ | friction factor |
| $\Delta\pi$ | osmotic pressure difference, Pa |
| $\rho$ | solution density, kg $m^{-3}$ |
| $\phi$ | osmotic coefficient |
| $\omega_n$ | friction factor fitting parameter |

*Subscripts*

| | |
|---|---|
| $b$ | bulk |
| $c$ | concentrated |
| $d$ | dilute |
| $i$ | inlet |

| | |
|---|---|
| $L$ | outlet |
| $m$ | membrane interface |

## References


[1] G.Z. Ramon, B.J. Feinberg, E.M.V. Hoek, Membrane-based production of salinity-gradient power, Energy Environ. Sci. 4 (2011) 4423–4434.
[2] B.E. Logan, M. Elimelech, Membrane-based processes for sustainable power generation using water, Nature 488 (2012) 313–319.
[3] J.W. Post, J. Veerman, H.V.M. Hamelers, G.J.W. Euverink, S.J. Metz, K. Nymeijer, C.J.N. Buisman, Salinity-gradient power: evaluation of pressure-retarded osmosis and reverse electrodialysis, J. Membr. Sci. 288 (2007) 218–230.
[4] J.W. Post, H.V.M. Hamelers, C.J.N. Buisman, Energy recovery from controlled mixing salt and fresh water with a reverse electrodialysis system, Environ. Sci. Technol. 42 (2008) 5785–5790.
[5] A. Achilli, T.Y. Cath, A.E. Childress, Power generation with pressure retarded osmosis: an experimental and theoretical investigation, J. Membr. Sci. 343 (2009) 42–52.
[6] P. Dlugolecki, A. Gambier, K. Nijmeijer, M. Wessling, Practical potential of reverse electrodialysis as process for sustainable energy generation, Environ. Sci. Technol. 43 (2009) 6888–6894.
[7] N.Y. Yip, M. Elimelech, Thermodynamic and energy efficiency analysis of power generation from natural salinity gradients by pressure retarded osmosis, Environ. Sci. Technol. 46 (2012) 5230–5239.
[8] B.J. Feinberg, G.Z. Ramon, E.M. Hoek, Thermodynamic analysis of osmotic energy recovery at a reverse osmosis desalination plant, Environ. Sci. Technol. 47 (2013) 2982–2989.
[9] F. Helfer, C. Lemckert, Y.G. Anissimov, Osmotic power with pressure retarded osmosis: theory, performance and trends – a review, J. Membr. Sci. 453 (2014) 337–358.
[10] J. Veerman, M. Saakes, S.J. Metz, G.J. Harmsen, Reverse electrodialysis: a validated process model for design and optimization, Chem. Eng. J. 166 (2011) 256–268.
[11] D.A. Vermaas, J. Veerman, N.Y. Yip, M. Elimelech, M. Saakes, K. Nijmeijer, High efficiency in energy generation from salinity gradients with reverse electrodialysis, ACS Sustain. Chem. Eng. 1 (2013) 1295–1302.
[12] S. Kim, E. Hoek, Modeling concentration polarization in reverse osmosis processes, Desalination 186 (2005) 111–128.
[13] L. Song, S. Hong, J. Hu, S. Ong, W. Ng, Simulations of full-scale reverse osmosis membrane process, J. Environ. Eng. 128 (2002) 960–966.
[14] L. Song, S. Yu, Concentration polarization in cross-flow reverse osmosis, AIChE J. 45 (1999) 921–928.
[15] W. Zhou, L. Song, T.K. Guan, A numerical study on concentration polarization and system performance of spiral wound RO membrane modules, J. Membr. Sci. 271 (2006) 38–46.
[16] E.M.V. Hoek, J. Allred, T. Knoell, B.-H. Jeong, Modeling the effects of fouling on full-scale reverse osmosis processes, J. Membr. Sci. 314 (2008) 33–49.
[17] G. Guillen, E.M.V. Hoek, Modeling the impacts of feed spacer geometry on reverse osmosis and nanofiltration processes, Chem. Eng. J. 149 (2009) 221–231.
[18] W.J. Hamer, Y.C. Wu, Osmotic coefficients and mean activity coefficients of uni-univalent electrolytes in water at 25 °C, J. Phys. Chem. Ref. Data 1 (1972) 1047–1100.
[19] K.S. Pitzer, J.C. Peiper, R. Busey, Thermodynamic properties of aqueous sodium chloride solutions, J. Phys. Chem. Ref. Data 13 (1984) 1–102.
[20] N.Y. Yip, A. Tiraferri, W.A. Phillip, J.D. Schiffman, L.A. Hoover, Y.C. Kim, M. Elimelech, Thin-film composite pressure retarded osmosis membranes for sustainable power generation from salinity gradients, Environ. Sci. Technol. 45 (2011) 4360–4369.
[21] J. Veerman, R.M. de Jong, M. Saakes, S.J. Metz, G.J. Harmsen, Reverse electrodialysis: comparison of six commercial membrane pairs on the thermodynamic efficiency and power density, J. Membr. Sci. 343 (2009) 7–15.
[22] APMonitor, ⟨http://apmonitor.com/⟩.
[23] Y.C. Kim, Y. Kim, D. Oh, K.H. Lee, Experimental Investigation of a spiral-wound pressure-retarded osmosis membrane module for osmotic power generation, Environ. Sci. Technol. 47 (2013) 2966–2973.
[24] T.Y. Cath, M. Elimelech, J.R. McCutcheon, R.L. McGinnis, A. Achilli, D. Anastasio, A.R. Brady, A.E. Childress, I.V. Farr, N.T. Hancock, Standard methodology for evaluating membrane performance in osmotically driven membrane processes, Desalination 312 (2012) 31–38.
[25] S. Loeb, Large-scale power production by pressure-retarded osmosis, using river water and sea water passing through spiral modules, Desalination 143 (2002) 115–122.
[26] S. Loeb, One hundred and thirty benign and renewable megawatts from Great Salt Lake? The possibilities of hydroelectric power by pressure-retarded osmosis, Desalination 141 (2001) 85–91.
[27] A. Tiraferri, N. Yin Yip, A.P. Straub, S. Romero-Vargas Castrillon, M. Elimelech, A method for the simultaneous determination of transport and structural parameters of forward osmosis membranes, J. Membr. Sci. 444 (2013) 523–538.